

The role of europium and dysprosium in the bluish-green long lasting $\text{Sr}_2\text{Al}_2\text{SiO}_7:\text{Eu}^{2+}$, Dy^{3+} phosphor by solid state reaction method

Ishwar Prasad Sahu¹

Received: 3 May 2015 / Accepted: 5 June 2015 / Published online: 21 June 2015
© Springer Science+Business Media New York 2015

Abstract The $\text{Sr}_2\text{Al}_2\text{SiO}_7$; $\text{Sr}_2\text{Al}_2\text{SiO}_7:\text{Eu}^{2+}$; $\text{Sr}_2\text{Al}_2\text{SiO}_7:\text{Dy}^{3+}$ and $\text{Sr}_2\text{Al}_2\text{SiO}_7:\text{Eu}^{2+}$, Dy^{3+} phosphors were synthesized by the traditional high temperature solid state reaction method. The synthesized phosphors were characterized by powder X-ray diffraction, energy dispersive X-ray spectroscopy, thermoluminescence (TL), photoluminescence (PL) long afterglow and mechanoluminescence (ML) techniques. The crystal structures of sintered phosphors were gehlenite type structure which belongs to the tetragonal crystallography. The TL properties of these phosphors were investigated and results were also compared. Under the ultraviolet excitation, the emission spectra of $\text{Sr}_2\text{Al}_2\text{SiO}_7:\text{Eu}^{2+}$ and $\text{Sr}_2\text{Al}_2\text{SiO}_7:\text{Eu}^{2+}$, Dy^{3+} phosphors were composed of a broad band peaking at 490 nm (bluish-green), belonging to the broad emission band and $\text{Sr}_2\text{Al}_2\text{SiO}_7:\text{Dy}^{3+}$ phosphor emits the white light, which was confirmed from the calculated CIE coordinates. When the $\text{Sr}_2\text{Al}_2\text{SiO}_7:\text{Eu}^{2+}$ phosphor is co-doped with Dy^{3+} , the intensity of TL, PL, afterglow and ML is strongly enhanced. Decay graph indicate that both the sintered phosphors contains fast decay and slow decay process. The ML intensities of $\text{Sr}_2\text{Al}_2\text{SiO}_7:\text{Dy}^{3+}$; $\text{Sr}_2\text{Al}_2\text{SiO}_7:\text{Eu}^{2+}$ and $\text{Sr}_2\text{Al}_2\text{SiO}_7:\text{Eu}^{2+}$, Dy^{3+} phosphors were proportionally increased with the increasing impact velocity of the moving piston, which suggests that these phosphor can be used as sensors to detect the stress of an object.

1 Introduction

In order to conserve natural resources, solar energy is one of the possible endless sources available. Long afterglow (persistence) phosphors store the absorbed energy and release of the energy occurs with a delay [1]. The absorption of energy can occur in the UV or visible region of the electromagnetic spectrum and the emission occurs in the visible region. If afterglow persists for a longer duration, then the phosphors is known as long afterglow phosphors. [2, 3]. It is generally believed that the persistent luminescence of materials involves luminescence centers and trap centers. Charge carriers are generated by the excitation in the luminescence centers and then trapped in the trap centers subsequently. Their de-trapping is thermally activated, which can cause a delay in the spectral emission, causing the persistent luminescence [4, 5]. Long afterglow phosphors find application in displays, lighting devices, traffic signs, emergency signages, textile printing, decorations and watch dials, etc. where one can see the objects clearly even in the dark. The afterglow can be improved by the addition of radioisotopes such as tritium and promethium. The addition of radioisotopes is environmentally unsafe and this makes it necessary to find alternate afterglow phosphors that are free from radioisotopes [6]. At present there is a demand for stable colors with a long, bright afterglow and a lot of researches are being conducted in this area [7, 8].

Alkaline earth (Sr, Ca, Ba) silicates have attracted much attention and become an interesting topic in the field of luminescent materials because of their high chemical stability and water resistant property, by comparing with sulfide and aluminates phosphors [9–11]. Therefore, the preparation of persistent phosphors with better water resistance is an important requirement. However, the

✉ Ishwar Prasad Sahu
ishwarprasad1986@gmail.com

¹ School of Studies in Physics and Astrophysics, Pt. Ravishankar Shukla University, Raipur 492010, CG, India

research of silicate based long afterglow materials has been developed several years ago and the study mainly concentrates on the alkaline earth silicate host [12, 13].

Over the last two decades, considerable attention has been paid to the synthesis, structural and optical studies of melilite type ceramics [14]. An akermanite ($A_2MgSi_2O_7$) and gehlenite ($A_2Al_2SiO_7$) are the two members of melilite group where $A = Ca$ or Sr . They have tetragonal crystal structure with space group $P\bar{4}2_1m$ (no. 113) [15, 16]. These materials also have the properties of strong triboluminescence [mechanoluminescence (ML)] and thermoluminescence (TL) [17]. Currently, the ML phenomenon has attracted more attention because of its potential application for sensing structural damage, fractures and deformation [18, 19]. Many efforts have been devoted to developing ML sensors due to their various applications such as visualization of stress, damage detection for air planes or cars, and the study of human diseases in the near future [20–22].

In this paper, strontium alumino-silicate was chosen as the host due to its special properties, such as low cost, easy preparation, excellent thermal and chemical stabilities, and especially the strong absorption in the near-UV region. The mechanism of long afterglow phosphors, especially $Sr_2Al_2SiO_7:Eu^{2+}$, Dy^{3+} phosphors processes are still unclear. In order to understand overall mechanism, the roles of Eu^{2+} and Dy^{3+} in $Sr_2Al_2SiO_7$ phosphor have been studied in details. The study of the structural characterization is carried out on the basis of X-ray diffraction (XRD) and energy dispersive X-ray spectroscopy (EDX). The luminescence studies were investigated on the basis of TL glow curve, PL spectra, CIE chromaticity diagram, long afterglow and ML properties.

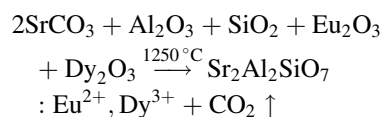
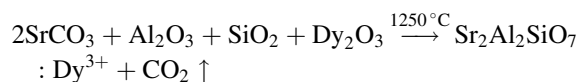
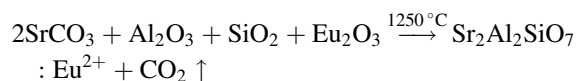
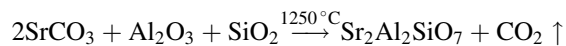
2 Experimental

2.1 Synthesis

The solid state reaction method is commonly used for synthesis of luminescent materials at elevated temperatures. During the synthesis of phosphors, a host matrix is formed from high purity starting chemicals and the impurities, also known as activators and co-activators of specified quantities are diffused into the crystal lattice. The formation of a phosphor host and doping process by solid solution is critical and is highly dependent on the reaction temperature and the environmental conditions [23].

The powder samples of $Sr_2Al_2SiO_7$; $Sr_2Al_2SiO_7:Eu^{2+}$; $Sr_2Al_2SiO_7:Dy^{3+}$ and $Sr_2Al_2SiO_7:Eu^{2+}$, Dy^{3+} phosphors were prepared by the high temperature solid state reaction method. The starting materials were strontium carbonate

[$SrCO_3$ (99.95 %)], aluminium oxide [Al_2O_3 (99.98 %)], silicon di-oxide [SiO_2 (99.99 %)], europium oxide (0.01 mol%) [Eu_2O_3 (99.99 %)] and dysprosium oxide (0.03 mol%) [Dy_2O_3 (99.99 %)], all of analytical grade, were employed in this experiment. A small amount (0.3 mol%) of boric acid [H_3BO_3 (99.99 %)] was added as flux. Initially, the raw materials were weighed according to the nominal compositions of phosphors and then the powders were mixed and milled thoroughly for 2 h using the agate mortar and pestle. The chemical reaction used for stoichiometric calculation is:



The ground sample are placed in an alumina crucible and subsequently fired at 1250 °C for 3 h in a weak reducing atmosphere excepting $Sr_2Al_2SiO_7$ and $Sr_2Al_2SiO_7:Dy^{3+}$ phosphors. The weak reducing atmosphere was generated with the help of activated carbon. At last the nominal compounds were obtained after the cooling down of the programmable furnace and products were finally ground into powder for characterizing the phosphors.

2.2 Instrumentation techniques

The powder XRD pattern has been obtained by Bruker D8 advanced X-ray powder diffractometer using $CuK\alpha$ radiation (1.54060 Å) and the data were collected over the 2θ range 10°–70° at room temperature. An EDX spectrum was used for the elemental (qualitative and quantitative) analysis of the prepared phosphors. TL glow curves were recorded with the help of TLD reader 1009I by Nucleonix (Hyderabad, India Pvt. Ltd.) at linear heating rate of 5 °C s⁻¹ after irradiation using a 365 nm UV radiation for 10 min. The excitation and emission spectra were recorded by RF 5301 PC spectrofluorophotometer by SHIMADZU using the Xenon lamp (365 nm) as excitation source when measuring. The (long afterglow) decay curve was obtained using a Perkin Elmer fluorescent spectrometer with the proper excitation under a UV lamp (365 nm). The ML measurement was observed by the home made lab system comprising of an RCA-931A photomultiplier tube (PMT). The ML glow curve can be plotted with the help of SM-340

application software installed in a computer attached with the storage oscilloscope. All the measurements were performed at room temperature.

3 Results and discussion

3.1 XRD analysis

In order to determine the crystal structure, powder XRD analysis has been carried out. The typical XRD patterns of $\text{Sr}_2\text{Al}_2\text{SiO}_7$; $\text{Sr}_2\text{Al}_2\text{SiO}_7:\text{Eu}^{2+}$; $\text{Sr}_2\text{Al}_2\text{SiO}_7:\text{Dy}^{3+}$ and $\text{Sr}_2\text{Al}_2\text{SiO}_7:\text{Eu}^{2+}, \text{Dy}^{3+}$ phosphors with that of the standard JCPDS file are shown in Fig. 1. Nearly, all the diffraction peaks of the resultant phosphors are consistent with Joint Committee Powder Diffraction Standard data (JCPDS) file (JCPDS: 75-1234) [24]. The position and intensity of diffraction peaks of $\text{Sr}_2\text{Al}_2\text{SiO}_7$; $\text{Sr}_2\text{Al}_2\text{SiO}_7:\text{Eu}^{2+}$; $\text{Sr}_2\text{Al}_2\text{SiO}_7:\text{Dy}^{3+}$ and $\text{Sr}_2\text{Al}_2\text{SiO}_7:\text{Eu}^{2+}, \text{Dy}^{3+}$ phosphors were well matched with the standard JCPDS file. The crystal

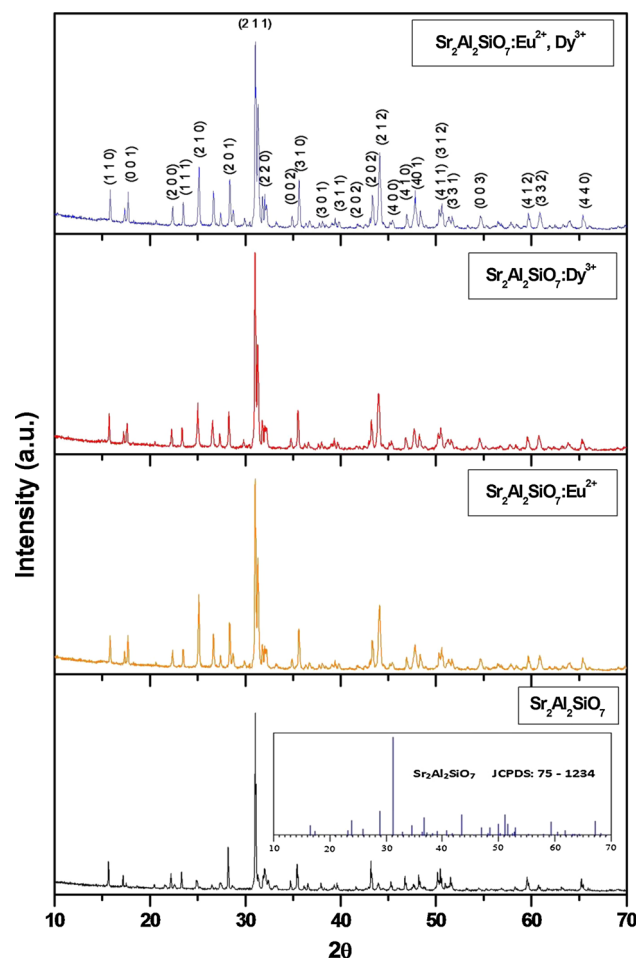


Fig. 1 XRD pattern of $\text{Sr}_2\text{Al}_2\text{SiO}_7$; $\text{Sr}_2\text{Al}_2\text{SiO}_7:\text{Eu}^{2+}$; $\text{Sr}_2\text{Al}_2\text{SiO}_7:\text{Dy}^{3+}$ and $\text{Sr}_2\text{Al}_2\text{SiO}_7:\text{Eu}^{2+}, \text{Dy}^{3+}$ phosphors

structure of all the sintered $\text{Sr}_2\text{Al}_2\text{SiO}_7$; $\text{Sr}_2\text{Al}_2\text{SiO}_7:\text{Eu}^{2+}$; $\text{Sr}_2\text{Al}_2\text{SiO}_7:\text{Dy}^{3+}$ and $\text{Sr}_2\text{Al}_2\text{SiO}_7:\text{Eu}^{2+}, \text{Dy}^{3+}$ phosphors were gelhenite type structure which belongs to the tetragonal crystallography with space group $P4_21m$, this structure is a member of the melilite group and forms a layered compound.

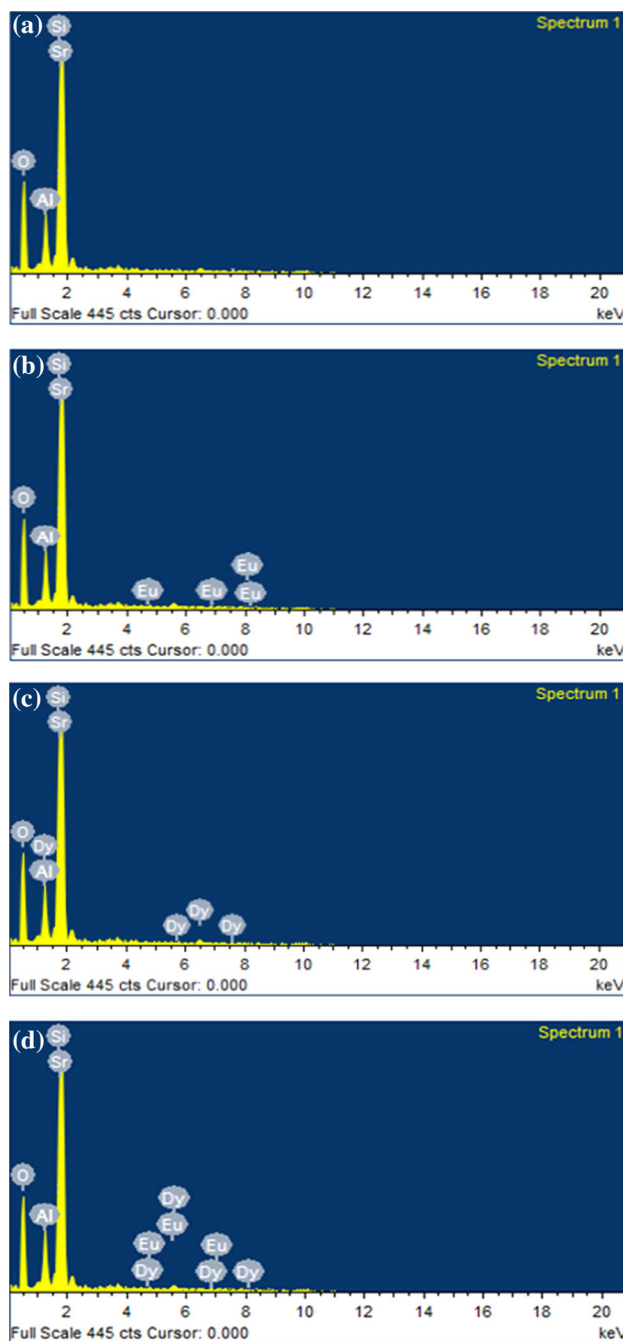


Fig. 2 a EDX spectra of $\text{Sr}_2\text{Al}_2\text{SiO}_7$ phosphor. b EDX spectra of $\text{Sr}_2\text{Al}_2\text{SiO}_7:\text{Eu}^{2+}$ phosphor. c EDX spectra of $\text{Sr}_2\text{Al}_2\text{SiO}_7:\text{Dy}^{3+}$ phosphor. d EDX spectra of $\text{Sr}_2\text{Al}_2\text{SiO}_7:\text{Eu}^{2+}, \text{Dy}^{3+}$ phosphor

Table 1 Chemical composition of $\text{Sr}_2\text{Al}_2\text{SiO}_7$; $\text{Sr}_2\text{Al}_2\text{SiO}_7:\text{Eu}^{2+}$; $\text{Sr}_2\text{Al}_2\text{SiO}_7:\text{Dy}^{3+}$ and $\text{Sr}_2\text{Al}_2\text{SiO}_7:\text{Eu}^{2+}$, Dy^{3+} phosphors

(a) $\text{Sr}_2\text{Al}_2\text{SiO}_7$				(b) $\text{Sr}_2\text{Al}_2\text{SiO}_7:\text{Eu}^{2+}$			
Sr. no.	Elements	Atomic (%)	Weight (%)	Sr. no.	Elements	Atomic (%)	Weight (%)
1	O K	40.75	63.89	1	O K	39.85	63.76
2	Al K	9.53	11.77	2	Al K	8.96	10.61
3	Si K	8.73	9.68	3	Si K	8.89	9.75
4	Sr L	40.88	14.65	4	Sr L	39.56	14.24
Total		99.99	99.99	5	Eu L	2.73	1.63
				Total		99.99	99.99
(c) $\text{Sr}_2\text{Al}_2\text{SiO}_7:\text{Dy}^{3+}$				(d) $\text{Sr}_2\text{Al}_2\text{SiO}_7:\text{Eu}^{2+}$, Dy^{3+}			
Sr. no.	Elements	Atomic (%)	Weight (%)	Sr. no.	Elements	Atomic (%)	Weight (%)
1	O K	40.51	62.46	1	O K	39.20	62.91
2	Al K	8.92	10.61	2	Al K	8.87	10.33
3	Si K	8.23	9.58	3	Si K	8.54	9.53
4	Sr L	39.83	13.70	4	Sr L	38.72	13.58
5	Dy L	2.51	3.65	5	Eu L	1.78	1.39
Total		99.99	99.99	6	Dy L	2.89	2.25
				Total		99.99	99.99

3.2 Energy dispersive X-ray spectroscopy (EDX)

Figure 2a, b, c, d shows the EDX spectra of $\text{Sr}_2\text{Al}_2\text{SiO}_7$; $\text{Sr}_2\text{Al}_2\text{SiO}_7:\text{Eu}^{2+}$; $\text{Sr}_2\text{Al}_2\text{SiO}_7:\text{Dy}^{3+}$ and $\text{Sr}_2\text{Al}_2\text{SiO}_7:\text{Eu}^{2+}$, Dy^{3+} phosphors. The composition of the powder sample has been measured using EDX. Table 1 shows the compositional elements of $\text{Sr}_2\text{Al}_2\text{SiO}_7$; $\text{Sr}_2\text{Al}_2\text{SiO}_7:\text{Eu}^{2+}$; $\text{Sr}_2\text{Al}_2\text{SiO}_7:\text{Dy}^{3+}$ and $\text{Sr}_2\text{Al}_2\text{SiO}_7:\text{Eu}^{2+}$, Dy^{3+} phosphors. EDX is a standard procedure for identifying and quantifying elemental composition of sample area as small as a few nanometers. They appear no other emissions apart from strontium (Sr), aluminium (Al), silicon (Si) and oxygen (O) in $\text{Sr}_2\text{Al}_2\text{SiO}_7$ phosphor; strontium (Sr), aluminium (Al), silicon (Si), oxygen (O) and europium (Eu) in $\text{Sr}_2\text{Al}_2\text{SiO}_7:\text{Eu}^{2+}$ phosphor; strontium (Sr), aluminium (Al), silicon (Si), oxygen (O) and dysprosium (Dy) in $\text{Sr}_2\text{Al}_2\text{SiO}_7:\text{Dy}^{3+}$ phosphor; strontium (Sr), aluminium (Al), silicon (Si), oxygen (O), europium (Eu) and dysprosium (Dy) in $\text{Sr}_2\text{Al}_2\text{SiO}_7:\text{Eu}^{2+}$, Dy^{3+} phosphor; EDX spectra of the samples. In the spectrum intense peaks are present which confirm the presence of elements in $\text{Sr}_2\text{Al}_2\text{SiO}_7$; $\text{Sr}_2\text{Al}_2\text{SiO}_7:\text{Eu}^{2+}$; $\text{Sr}_2\text{Al}_2\text{SiO}_7:\text{Dy}^{3+}$ and $\text{Sr}_2\text{Al}_2\text{SiO}_7:\text{Eu}^{2+}$, Dy^{3+} phosphors.

3.3 Thermoluminescence (TL)

Thermally stimulated luminescence (TSL) is observed when a phosphor with deep traps is excited with UV for a while at rather low temperatures and then heated, due to the recombination of electrons thermally reactivated from the

deep traps. Such an emission is also referred to as TL. Irradiation with α -rays, β -rays, γ -rays, UV-rays or X-rays transfers electrons and holes to their respective traps [25]. TL measurements provide information concerning the trap levels. In order to obtain information about luminescence process of phosphors and to apply them in various fields, the knowledge of defects or traps and their location in the band gap of materials is very important. The temperature dependence of the emission intensity is called the glow curve [26]. The excitation energy partly does the work of moving electrons to traps. Some of these electrons are trapped and locate themselves at a depth (activation energy E) below the conduction band. The trap levels or centers play a significant role in energy storage for persistent photo-luminescent and thermo-luminescent phosphors. This radiation energy stored in the form of trapped electrons is released by raising the temperature of the material and the released energy is converted to luminescence [27, 28].

Figure 3 shows the TL glow curve of $\text{Sr}_2\text{Al}_2\text{SiO}_7$, $\text{Sr}_2\text{Al}_2\text{SiO}_7:\text{Eu}^{2+}$, $\text{Sr}_2\text{Al}_2\text{SiO}_7:\text{Dy}^{3+}$ and $\text{Sr}_2\text{Al}_2\text{SiO}_7:\text{Eu}^{2+}$, Dy^{3+} phosphors with fixed UV irradiation (10 Minute) time at constant heating rate 5°C s^{-1} . Every time for the TL measurement, the quantity of the powder samples were kept fixed (8 mg). The TL peak of $\text{Sr}_2\text{Al}_2\text{SiO}_7$ is very weak and can be neglected. The TL glow peaks were occurred at 82.59, 113.98 and 97.23 $^\circ\text{C}$ for $\text{Sr}_2\text{Al}_2\text{SiO}_7:\text{Eu}^{2+}$; $\text{Sr}_2\text{Al}_2\text{SiO}_7:\text{Dy}^{3+}$ and $\text{Sr}_2\text{Al}_2\text{SiO}_7:\text{Eu}^{2+}$, Dy^{3+} phosphors respectively. Correspondingly, the depth of the traps is estimated to be the 0.58, 0.80 and 0.70 eV. The locations of the glow

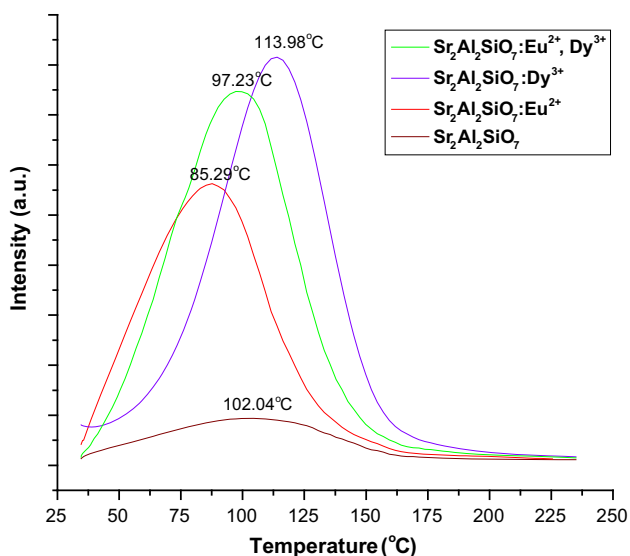


Fig. 3 Comparatively TL glow curve of $\text{Sr}_2\text{Al}_2\text{SiO}_7$; $\text{Sr}_2\text{Al}_2\text{SiO}_7$: Eu^{2+} ; $\text{Sr}_2\text{Al}_2\text{SiO}_7$: Dy^{3+} and $\text{Sr}_2\text{Al}_2\text{SiO}_7$: Eu^{2+} , Dy^{3+} phosphors for 10 min UV irradiation time

peaks indicate that the sequence of the trap depth should be $\text{Sr}_2\text{Al}_2\text{SiO}_7$: Eu^{2+} < $\text{Sr}_2\text{Al}_2\text{SiO}_7$: Eu^{2+} , Dy^{3+} < $\text{Sr}_2\text{Al}_2\text{SiO}_7$: Dy^{3+} ; because the higher temperature the peak locates, the greater activation energy is needed for de-trapping. The glow intensity has the similar sequence. Moreover, the intensities of $\text{Sr}_2\text{Al}_2\text{SiO}_7$: Eu^{2+} , Dy^{3+} < $\text{Sr}_2\text{Al}_2\text{SiO}_7$: Dy^{3+} are much stronger than that of $\text{Sr}_2\text{Al}_2\text{SiO}_7$: Eu^{2+} indicating that the formers have a higher ability of trapping carriers.

As is well known, the existence of suitable charge traps in host lattice is responsible for long lasting phosphorescence. On the mechanism of long afterglow, it is a common viewpoint that during the excitation period the energy of incident light is partly stored in the form of captured charges; those captured charges can be thermally released from the traps at room temperature to result in the characteristic emission of the luminescence ion. Because the release of the captured electrons is durative, the luminescence of the materials shows the property of long life [29–31]. From TL glow curve, the peak position of $\text{Sr}_2\text{Al}_2\text{SiO}_7$: Eu^{2+} phosphor occurred at low temperature, which is closely related to the depth of the trap levels. If the depth of the trap levels is too shallow, trapped charges will easily release from the traps and the phosphor will show a rapid decay of its thermal luminescence at low temperature [low activation energy (0.58 eV) is require]. On the case of $\text{Sr}_2\text{Al}_2\text{SiO}_7$: Dy^{3+} phosphors, the depth of the trap level is too deep, charges will remain in the trap and high activation energy (0.80 eV) is require, which is difficult to obtain at room temperature, hence the phosphor will not show afterglow at room temperature. The optimum trap depth for the silicate and aluminate based phosphors is in the range

of 0.65–0.75 eV which is suitable for the thermal release at room temperature to show long afterglow. In the case of $\text{Sr}_2\text{Al}_2\text{SiO}_7$: Eu^{2+} , Dy^{3+} phosphor the depth of trap is 0.70 eV, which is a sign of a good persistence luminescent material.

In $\text{Sr}_2\text{Al}_2\text{SiO}_7$: Eu^{2+} phosphor, Eu^{2+} will replace the site of Sr^{2+} because they have similar ionic radius [Sr^{2+} (1.12 Å), Eu^{2+} (1.12 Å) and Dy^{3+} (0.99 Å)], and due to the different electro-negativity of the two ions, the replacement will produce traps in the host. In Dy^{3+} doped sample, Dy^{3+} replacing Sr^{2+} will result in defects with positive charge in the host and should capture electrons, i.e., the most probable defects created by Dy^{3+} replacement may be electronic traps. The experimental results indicate that the role of Eu^{2+} in $\text{Sr}_2\text{Al}_2\text{SiO}_7$: Eu^{2+} , Dy^{3+} is not only the luminescence center, but also a trap center, which capture the free electrons to form metastable state and then release the trapped electrons upon thermal activation to recombine with the luminescent centers accompanying the luminescence. On the other hand, Dy^{3+} ions could be not only as trap center, but also act as luminescence center.

3.4 Determination of kinetic parameters

Evaluation of kinetic parameters, i.e. the activation energy (E) of the traps involved in the TL emission, the order of kinetics (b), and the frequency factor (s), associated with the glow peaks of the TSL, is one of the most studied subjects in the field of condensed matter physics and a complete description of the thermoluminescent characteristics of a TL material requires to obtain these parameters. There are various methods for evaluating the trapping parameters from TL glow curves [32, 33] For example, when one of the glow peaks is highly isolated from the others, the experimental method such as peak shape method is a suitable method to determine them from the glow peak. The TL parameters i.e. activation energy, frequency factor and shape factor (μ_g), of the glow peaks of prepared phosphors were calculated using the peak shape method are shown in Table 2. [34] The relationship between the frequency factor ‘s’ and the activation energy ‘E’ is given by the Eq. (1)

$$\frac{\beta E}{kT_m^2} = s \left[1 + (b - 1) \frac{2kT_m}{E} \right] \exp(E/KT_m) \quad (1)$$

where, k is Boltzmann constant, E is activation energy, b is order of kinetics, T_m is temperature of peak position, and β is the heating rate. In the present work $\beta = 5 \text{ }^\circ\text{C s}^{-1}$. Trap depth for second order kinetics is calculated using the Eq. (2)

Table 2 Shape factor (μ_g), activation energy (E) and frequency factor (s^{-1}) for UV irradiated $Sr_2Al_2SiO_7:Eu^{2+}$; $Sr_2Al_2SiO_7:Dy^{3+}$ and $Sr_2Al_2SiO_7:Eu^{2+}, Dy^{3+}$ phosphors

Phosphors name	UV min	HTR	T_1 (°C)	T_m (°C)	T_2 (°C)	τ (°C)	δ (°C)	ω (°C)	$\mu_g = \delta/\omega$	Activation energy	Frequency factor
$Sr_2Al_2SiO_7:Eu^{2+}$	10	5	53.35	85.29	113.98	31.94	28.69	60.63	0.47	0.58	5.10×10^7
$Sr_2Al_2SiO_7:Dy^{3+}$	10	5	85.29	113.98	137.85	28.69	23.87	52.56	0.45	0.80	1.00×10^{10}
$Sr_2Al_2SiO_7:Eu^{2+}, Dy^{3+}$	10	5	66.19	97.23	120.57	31.04	23.34	54.38	0.43	0.70	1.36×10^8

$$E = 2kT_m \left(1.76 \frac{T_m}{\omega} - 1 \right) \quad (2)$$

where, ω is the total half width intensity $\omega = \tau + \delta$, τ is the half width at the low temperature side of the peak ($\tau = T_m - T_1$); δ is the half width towards the fall-off side of the glow peak ($\delta = T_2 - T_m$), and T_m is the peak temperature at the maximum. The shape factor $\mu_g = \delta/\omega$. The shape factor (μ_g) is to differentiate between first and second order TL glow peak. (μ_g) = 0.39–0.42 for the first order kinetics, (μ_g) = 0.43–0.48 for the mixed order kinetics and (μ_g) = 0.49–0.52 for the second order kinetics. [35–37].

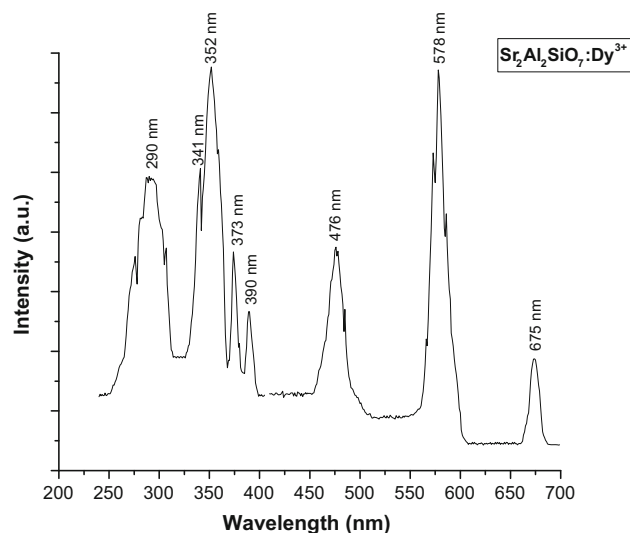
Shape factors (μ_g) range between 0.43 and 0.47, which indicates that it is a case of non-first order kinetics, approaching towards second order, responsible for deeper trap depth resulting in the long afterglow. The activation energy of $Sr_2Al_2SiO_7:Eu^{2+}, Dy^{3+}$ phosphor is found 0.70 eV which is a sign of a good persistence luminescent material. It is reported that a suitable trap depth (0.65–0.75 eV) is essential for phosphors to show long persistence [38], therefore, the trap depth of prepared phosphors is suitable for long afterglow (see Table 2).

3.5 Photoluminescence (PL)

When light of sufficient energy is incident on a material, photons are absorbed and electronic excitations are created. Eventually, these excitations relax and the electrons return to the ground state. If radiative relaxation occurs, the emitted light is called photoluminescence (PL). Various important material properties (physical and chemical) of materials by using photons to induce excited electronic states in the material system and analyzing the optical emission as these states relax.

3.6 $Sr_2Al_2SiO_7:Dy^{3+}$ phosphor

In order to study the luminescent properties of the phosphor, excitation and emission spectra of the prepared $Sr_2Al_2SiO_7:Dy^{3+}$ phosphor was recorded and shown in Fig. 4. The excitation spectra were observed in the range of 200–400 nm and emission spectra were recorded in the

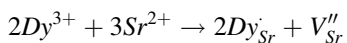
**Fig. 4** Photoluminescence spectra of $Sr_2Al_2SiO_7:Dy^{3+}$ phosphor

range of 400–700 nm. The excitation spectrum in the range 200–400 nm consists of the $f \rightarrow f$ transition of the Dy^{3+} ion. The excitation spectrum of $Sr_2Al_2SiO_7:Dy^{3+}$ phosphor shows strong excited peak at 352 nm and less intense excited peak at 290, 341, 373 and 390 nm, which are ascribed to the transitions from the ground state to excitation states in the $4f^9$ configuration of Dy^{3+} but not easy to be clearly assigned due to the dense and somewhat overlapped levels of $4f$ configuration of Dy^{3+} in the high energy region. When the $Sr_2Al_2SiO_7:Dy^{3+}$ phosphor was excited at 352 nm, simultaneous emissions of blue (476 nm), yellow (578 nm) and red (675 nm) peak were observed. Notice that the red emission is less intense than the blue and yellow emissions. These three different emission bands originated from the one origin owing to their having the same excitation wavelength [39]. The transitions involved in blue, yellow and red bands of Dy^{3+} ion are well known and have been identified as ${}^4F_{9/2} \rightarrow {}^6H_{15/2}$, ${}^4F_{9/2} \rightarrow {}^6H_{13/2}$ and ${}^4F_{9/2} \rightarrow {}^6H_{11/2}$ transitions respectively. One can also find that the emission lines of Dy^{3+} are broadened somewhat because there are several Stark levels for the ${}^4F_{9/2} \rightarrow {}^6H_J$ levels.

It is well known that the former weak blue emission at 476 nm (${}^4F_{9/2} \rightarrow {}^6H_{15/2}$) is corresponded to the magnetic

dipole transition, which hardly varies with the crystal field strength around Dy^{3+} . While the later stronger yellow emission at 578 nm (${}^4F_{9/2} \rightarrow {}^6H_{13/2}$) belongs to the hypersensitive forced electric dipole transition, which is strongly influenced by the outside surrounding environment. According to the Judd–Ofelt theory [5], when Dy^{3+} locates at a low symmetry local site (without inversion symmetry), a yellow emission according to the electric dipole transition (${}^4F_{9/2} \rightarrow {}^6H_{13/2}$) will be dominant. Conversely, a magnetic dipole transition (${}^4F_{9/2} \rightarrow {}^6H_{15/2}$) will predominate in the emission spectra, resulting in a strong blue emission. In our case [Fig. 4 (emission part)], the yellow emission (${}^4F_{9/2} \rightarrow {}^6H_{13/2}$) will dominate. The strong yellow emission is also beneficial to decrease the color temperature of the phosphor and generate warm white light emission. Moreover, the hardly perceptible transition (${}^4F_{9/2} \rightarrow {}^6H_{13/2}$) emission at 578 nm can be observed, which is also due to the disordered crystal field and is corresponding to the structural study. It is well known that the (${}^4F_{9/2} \rightarrow {}^6H_{13/2}$) transition is hypersensitive and therefore, its intensity strongly depends on the host, while the (${}^4F_{9/2} \rightarrow {}^6H_{15/2}$) transition is less sensitive to the host. The optical properties of the material are often influenced by the structure of the matrix and synthesis technique [40].

When trivalent metallic ions, such as Dy^{3+} are incorporated into a host lattice and substitute divalent metallic ions, the charge balancing is necessarily required. Due to these chemically nonequivalent substitutions, an excess of positive charge in the host lattice must be compensated. One possible way of charge compensation mechanism is that two Dy^{3+} ions replace three Sr^{2+} ions to balance the charge of these phosphors, which create two Dy'_{Sr} positive defects and one V''_{Sr} negative defect.



For $Sr_2Al_2SiO_7:Dy^{3+}$ the incorporation of alkali metal ions can neutralize the charge generated by Dy^{3+} substitution for Sr^{2+} , and thus stabilize the structure and enhance the luminescence. Dy^{3+} ions have been often used as codopants in the previously developed aluminate and silicate based materials. When divalent alkaline earth ions, such as Ba^{2+} , Ca^{2+} or Sr^{2+} , is substituted by trivalent Dy^{3+} in the alkaline earth silicates and aluminates, various defects can be induced due to the charge compensation mechanism [41].

However, in Dy^{3+} singly doped samples, which are in our current interest, Dy^{3+} is not only the supplier of traps but also an activator itself. A process of emitting the white light in $Sr_2Al_2SiO_7:Dy^{3+}$ phosphor is illustrated schematically in Fig. 5. After irradiation with the ultraviolet light (process numbered [1]), most of the excitation energy

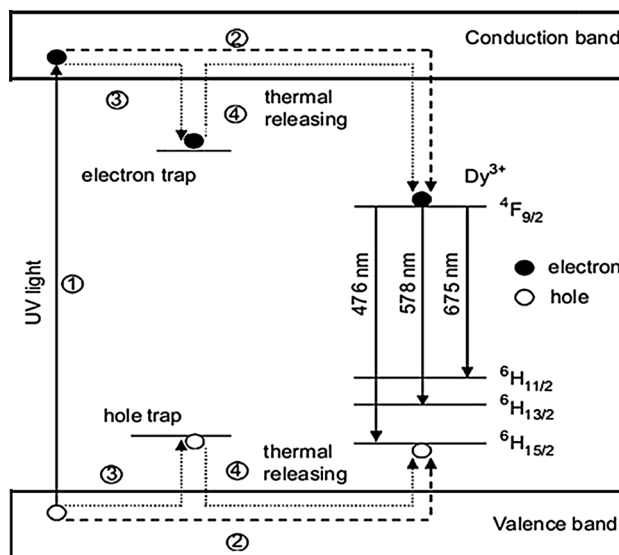


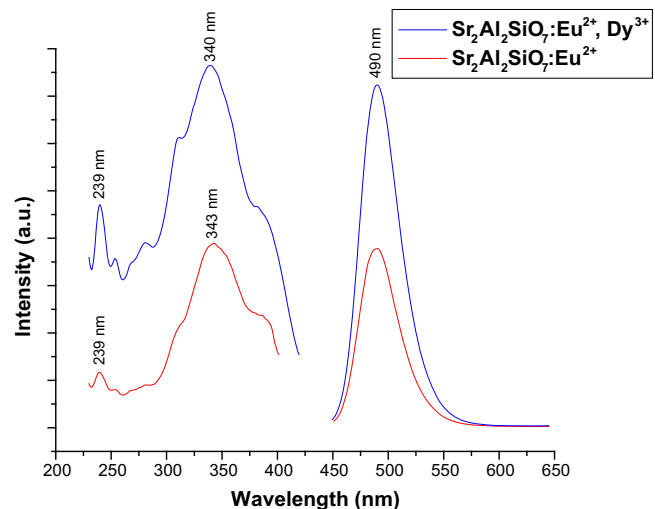
Fig. 5 Schematic diagram of the mechanism in $Sr_2Al_2SiO_7:Dy^{3+}$ phosphor

associated with the excited carriers (electrons or holes) will be transferred via the host directly to the luminescence centres Dy^{3+} , followed by the Dy^{3+} 4f emissions as the immediate luminescence (process [2]). However, part of the excitation energy will be stored when some of the excited carriers drop into the traps (process [3]), instead of returning to the ground states. Later, with thermal excitation at proper temperature, these carriers will be released from the traps and transferred via the host to the Dy^{3+} ions, followed by the characteristic Dy^{3+} emissions as long afterglow (process [4]). In the practical system, the electron traps and the hole traps may not be both equally abundant or important in terms of their contribution to the white light emission [42], as suggested in Fig. 5.

3.7 $Sr_2Al_2SiO_7:Eu^{2+}$ and $Sr_2Al_2SiO_7:Eu^{2+}, Dy^{3+}$ phosphors

The PL excitation and emission spectra of $Sr_2Al_2SiO_7:Eu^{2+}$ and $Sr_2Al_2SiO_7:Eu^{2+}, Dy^{3+}$ phosphors were shown in Fig. 6. A Xenon lamp with the 365 nm wavelength was utilized to excite the phosphors when measuring. The excitation spectra were observed in the range of 200–425 nm and emission spectra were recorded in the range of 400–650 nm. The results illustrate that both of them are broadband spectra. The excitation broad band due to transitions of Eu^{2+} between the ($4f^7$) ground state to the excited state $4f^65d^1$ [$(4f^7) \rightarrow 4f^65d^1$] configuration were observed under the ultra-violet (UV) excitation. As we could see from the Fig. 6, the excitation spectra of $Sr_2Al_2SiO_7:Eu^{2+}$ phosphors, it is seen that, two excitation peaks has been observed at 239 and 343 nm. Their

Fig. 6 PL spectra of $\text{Sr}_2\text{Al}_2\text{SiO}_7:\text{Eu}^{2+}$ and $\text{Sr}_2\text{Al}_2\text{SiO}_7:\text{Eu}^{2+}, \text{Dy}^{3+}$ phosphors



corresponding emission spectra were recorded at 490 nm, which emits the bluish-green color. From the excitation spectra of $\text{Sr}_2\text{Al}_2\text{SiO}_7:\text{Eu}^{2+}, \text{Dy}^{3+}$ phosphor, two peaks has been observed at 239 and 340 nm and their corresponding emission peak at about 490 nm, which also emits the bluish-green color. Although the 4f electrons of Eu^{2+} are not sensitive to crystal lattice environment due to the shielding function of outer shell, the 5d electrons can easily coupled with crystal lattice, thus the 4f5d hybridization state can be split by the influence of crystal field and coupled fiercely with crystal lattice phonon, which leads to a broad band emission. It is well known that the emission of Eu^{2+} ion in a solid-state compound generally shows a broad band character.

The emission peaks of both the prepared $\text{Sr}_2\text{Al}_2\text{SiO}_7:\text{Eu}^{2+}$ and $\text{Sr}_2\text{Al}_2\text{SiO}_7:\text{Eu}^{2+}, \text{Dy}^{3+}$ phosphors are similar and attributed to the typical emission of Eu^{2+} due to the $4f^65d^1 \rightarrow 4f^7$ transition, but there is no special emission of Eu^{3+} ions, while that of Eu^{3+} ion always gives a series of typical emission lines in a spectral region of 570–750 nm corresponding to its ${}^5\text{D}_0 \rightarrow {}^7\text{F}_J$ ($J = 1, 2, 3, 4$) transitions. This offers us a very convenient way to determine the valence state of europium ions in solid state compounds. The Eu^{3+} emission peak has not shown in the emission spectra, indicating that Eu^{3+} in the crystal matrix has been completely reduced to Eu^{2+} . From the $\text{Sr}_2\text{Al}_2\text{SiO}_7:\text{Eu}^{2+}, \text{Dy}^{3+}$ phosphor, co-doped Dy^{3+} did not emit any color [special Dy^{3+} emission peak are found at the 470 nm (blue region) and 577 nm (yellow region)] which indicates that neither direct excitation of Dy^{3+} nor energy transfer from Eu^{2+} to Dy^{3+} occurs in the $\text{Sr}_2\text{Al}_2\text{SiO}_7:\text{Eu}^{2+}, \text{Dy}^{3+}$ matrices crystal lattice. The co-doped Dy^{3+} playing a role as a hole trapped center at the holes trap levels, which capture the free electrons or holes when Eu^{2+} is excited and then release the free electrons or holes to the valence band.

However, the intensities of the emission bands are different. The strongest intensity could be obtained from Eu^{2+} doped and the Dy^{3+} co-doped $\text{Sr}_2\text{Al}_2\text{SiO}_7$ phosphor. With the only Eu^{2+} doped $\text{Sr}_2\text{Al}_2\text{SiO}_7$ phosphor, the intensity of the peak becomes smaller. In a word, the co-doping of Dy^{3+} ions has no influence to the position of the emission peak but the strong influence on the intensity of the emission. It is known that the bluish-green emission peaked at 490 nm corresponds to the transitions of ${}^4\text{F}_{9/2} \rightarrow {}^6\text{H}_{15/2, 13/2}$ this emission belongs to hypersensitive transition, which is strongly depended on outside environments of Dy^{3+} ions [43].

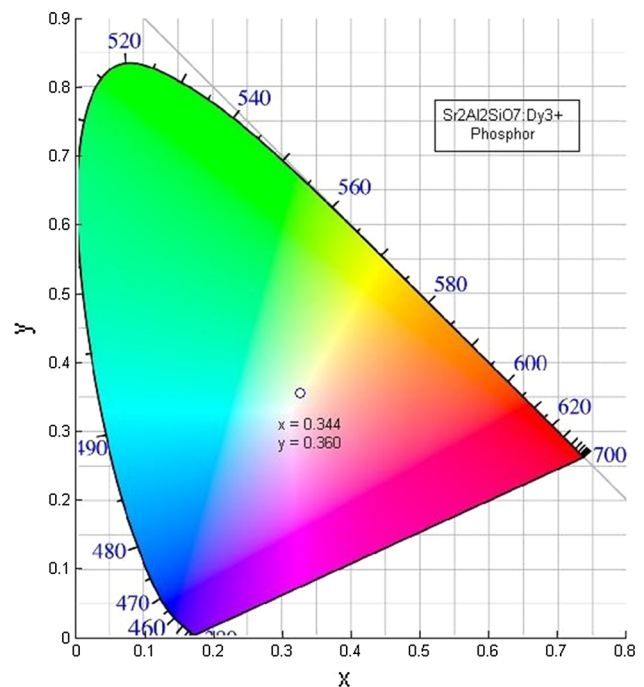


Fig. 7 CIE chromaticity diagram of $\text{Sr}_2\text{Al}_2\text{SiO}_7:\text{Dy}^{3+}$ phosphor

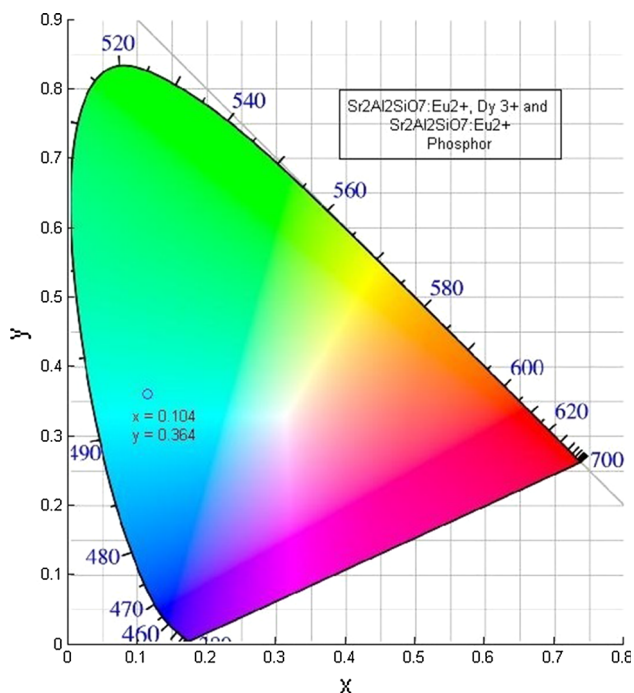


Fig. 8 CIE chromaticity diagram of Sr₂Al₂SiO₇:Eu²⁺ and Sr₂Al₂SiO₇:Eu²⁺, Dy³⁺ phosphors

3.8 CIE chromaticity coordinate

In general, color of any phosphor material is represented by means of color coordinates. Color coordinates are one of the important factors for evaluating phosphors' performance. In such case, the color coordinates of the Sr₂Al₂SiO₇:Dy³⁺ were calculated using the PL emission spectra data and the chromatic standard issued by the Commission Internationale de l'Eclairage in 1931 (CIE 1931) [44]. The CIE chromaticity diagram of Sr₂Al₂SiO₇:Dy³⁺ under 352 nm excitation is shown in Fig. 7 with the (o) symbol (x = 0.344, y = 0.360). It indicates that the color coordinates of present phosphors are very close to the "ideal white light" (x = 0.333, y = 0.333) in chromaticity diagram. In order to further improve the CIE color coordinates and achieve good quality white light emission, some other rare earth dopants, such as Ce³⁺, Eu²⁺, Eu³⁺, Tb³⁺, Tm³⁺, ions, emitting blue, green or red may need to be introduced into this phosphor system.

The color coordinates for the emission spectra were excited by 343 and 340 nm for the Sr₂Al₂SiO₇:Eu²⁺ and Sr₂Al₂SiO₇:Eu²⁺, Dy³⁺ phosphors and calculated by using the CIE are shown in Fig. 8. It is a well known fact that the color coordinates are same if the emission spectra profiles are identical. The calculated chromaticity coordinates of the Sr₂Al₂SiO₇:Eu²⁺ and Sr₂Al₂SiO₇:Eu²⁺, Dy³⁺ phosphors is given by (x = 0.104, y = 0.364), which is in agreement with the chromaticity coordinates of bluish-green color.

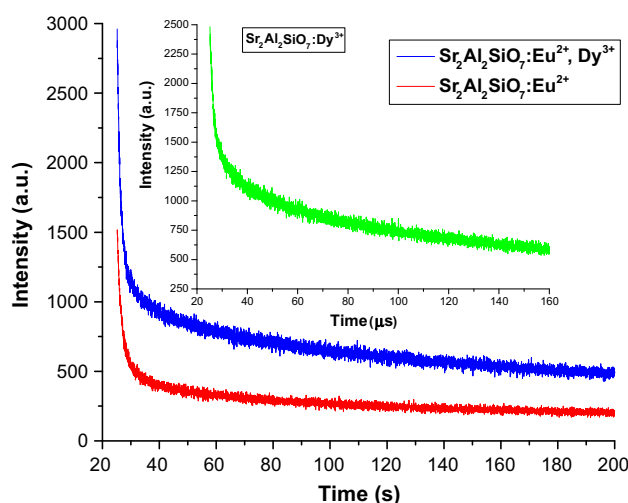


Fig. 9 Decay curves of Sr₂Al₂SiO₇:Eu²⁺ and Sr₂Al₂SiO₇:Eu²⁺, Dy³⁺ phosphors (inset—decay curves of Sr₂Al₂SiO₇:Dy³⁺ phosphor)

3.9 Long afterglow (decay)

Figure 9 shows the typical decay curves of Sr₂Al₂SiO₇:Eu²⁺ and Sr₂Al₂SiO₇:Eu²⁺, Dy³⁺ phosphors {(Inset—decay curves of Sr₂Al₂SiO₇:Dy³⁺ phosphor) The luminescence decay curve of Dy³⁺ doped Sr₂Al₂SiO₇ phosphor can be well fitted into a single exponential function as $I = I_0 \exp(-t/\tau)$ where, I_0 and I are the luminescence intensities at time 0 and t , respectively, and τ is the luminescence lifetime of the Dy³⁺ ion [45, 46]. The lifetime of Dy³⁺ is determined to be 41.66 μ s. Prior to the measurement, the samples were excited by a UV source for 2 min. Sr₂Al₂SiO₇:Eu²⁺ phosphor exhibits an obvious afterglow phenomenon. This demonstrates that traps which induce the afterglow have already existed even without Dy³⁺ doping. When the Sr₂Al₂SiO₇:Eu²⁺ phosphor is co-doped with Dy³⁺, the afterglow intensity is strongly enhanced. Furthermore, the duration of the afterglow is prolonged since the intensity of Sr₂Al₂SiO₇:Eu²⁺, Dy³⁺ is stronger than the Sr₂Al₂SiO₇:Eu²⁺ phosphor. The decay curves of the afterglow of the phosphors can be evaluated by the curve-fitting technique. The afterglow attenuates in the form of the exponential function. In this work, the double exponential equation which has been used widely can fit the experimental decay curves very well [43, 47–49].

$$I = A_1 \exp(-t/\tau_1) + A_2 \exp(-t/\tau_2) \quad (3)$$

where, I is phosphorescence intensity, A_1 , A_2 are constants, t is time, τ_1 and τ_2 are decay times (in second) for the exponential components. Decay curves are successfully fitted by the Eq. (3) and the fitting curve result are shown in Table 3. Using the fitting function provided by ORIGIN8 software, the calculated afterglow decay for the mentioned compounds was found. The results indicated that; both the phosphors show a rapid decay and the long-lasting phosphorescence.

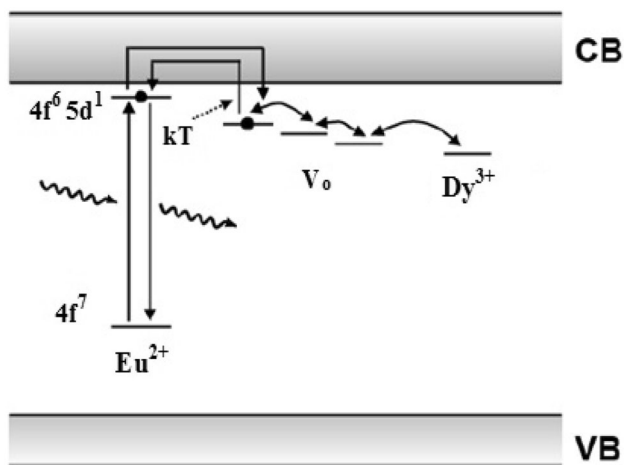
Table 3 Fitting results (decay curves) of the $\text{Sr}_2\text{Al}_2\text{SiO}_7:\text{Eu}^{2+}$ and $\text{Sr}_2\text{Al}_2\text{SiO}_7:\text{Eu}^{2+}, \text{Dy}^{3+}$ phosphors

Phosphor	τ_1 (s)	τ_2 (s)
$\text{Sr}_2\text{Al}_2\text{SiO}_7:\text{Eu}^{2+}$	1.48	51.29
$\text{Sr}_2\text{Al}_2\text{SiO}_7:\text{Eu}^{2+}, \text{Dy}^{3+}$	1.55	67.61

In general, the afterglow of phosphors is considered to be generated by the de-trapped carriers which recombine in the luminescent centers accompanied by the delay emission, hence the traps which induced by the lattice defects in phosphors play an important role on the afterglow. TL provides a possible method to investigate these traps. As shown in Fig. 3. $\text{Sr}_2\text{Al}_2\text{SiO}_7:\text{Eu}^{2+}$; $\text{Sr}_2\text{Al}_2\text{SiO}_7:\text{Dy}^{3+}$ and $\text{Sr}_2\text{Al}_2\text{SiO}_7:\text{Eu}^{2+}, \text{Dy}^{3+}$ phosphors present a broad TL band peaking at 82.59, 113.98 and 97.23 °C and their corresponding depth of trap is estimated to be 0.58, 0.80 and 0.70 eV respectively.

On the other hand, $\text{Sr}_2\text{Al}_2\text{SiO}_7:\text{Eu}^{2+}$ also exhibits an afterglow phenomenon, indicating that a trap has already existed in the matrix. The probably lattice defect responsible for this trap is the oxygen vacancies, induced by the lack of oxygen when the samples are sintered in reducing atmosphere. The oxygen vacancies may be attracted by Eu^{2+} ions because when Eu^{2+} replaces Sr^{2+} in the matrix, the local ionization potential decreases. Thereby oxygen vacancy becomes an electron trap in vicinity. The presence of Dy^{3+} reinforces the influence of Eu^{2+} on oxygen vacancy. In $\text{Sr}_2\text{Al}_2\text{SiO}_7:\text{Eu}^{2+}$ matrix, Dy^{3+} seems to have a great influence [50].

The co-doped Dy^{3+} acts as trap centers in silicates that trap the electrons generated during the exposure of phosphor to excitation source. The mechanism of afterglow in silicate based phosphor has been explained by many researchers and Aitasalo et al. [50] described a mechanism for persistent luminescence that incorporates suggestions from both Clabau and Dorenbos (Fig. 10) may be elaborated as: on receiving exposure to excitation source, an

**Fig. 10** Mechanism of persistent luminescence in $\text{Sr}_2\text{Al}_2\text{SiO}_7:\text{Eu}^{2+}, \text{Dy}^{3+}$ phosphor

electron of Eu^{2+} ($4f^7$) is promoted to the $4f^6 5d^1$ band followed by either direct or phonon assisted escape of the electron from Eu^{2+} to the host conduction band. The lattice defects close to the bottom of the host conduction band traps the electrons. Huge numbers of electrons are trapped by the traps assisted by Dy^{3+} at various depths making an important role of Dy^{3+} during the long afterglow. After the removal of excitation source, the captured electrons near the host conduction band released to the conduction band with thermal energy and consequent recombination of them with the emitting Eu^{2+} centers lead the persistent afterglow. Thus, the major cause for the afterglow is the number of electrons captured in the traps and its depths from the bottom of the conduction band of host material [51].

The activation energy of $\text{Sr}_2\text{Al}_2\text{SiO}_7:\text{Eu}^{2+}, \text{Dy}^{3+}$ phosphor is found 0.70 eV which is a sign of a good persistence luminescent material. It is reported that a suitable trap depth (0.65–0.75 eV) is essential for phosphors to show long persistence, therefore, the trap depth of prepared phosphor is suitable for long afterglow.

3.10 Mechanoluminescence (ML)

ML (also known as Triboluminescence) is an important physical phenomenon where an emission of light is observed due to mechanical deformation of materials, when they are subjected to some mechanical stress like rubbing, cleavage, compressing, impulsive deformation, crushing, grinding, shaking etc. [35, 36]. This phenomenon has been observed in many kinds of solids including ionic crystals, semiconductors, metals, glasses and organic crystals. In the present ML studies, an impulsive deformation technique has been used. When a load (moving piston) is applied on to the phosphor, initially the ML intensity increases with time, attains a peak value and then it decreases with time. Such a curve between the ML intensity and deformation time of a solid is known as the ML glow curve. During the deformation of a solid, a great number of physical processes may occur within very short time intervals, which may excite or stimulate the process of photon emission [52, 53].

Figure 11a, b, c, d shows that characteristics ML glow curve between peak ML intensity versus time for different heights of moving piston. The experiment was carried out for a fixed moving piston (400 gm, cylindrical shape) dropped with different heights. Every time for the ML measurement, the quantity of the powder sample is fixed (8 mg) and takes the fresh sample for observation. The sintered $\text{Sr}_2\text{Al}_2\text{SiO}_7$; $\text{Sr}_2\text{Al}_2\text{SiO}_7:\text{Eu}^{2+}$; $\text{Sr}_2\text{Al}_2\text{SiO}_7:\text{Dy}^{3+}$ and $\text{Sr}_2\text{Al}_2\text{SiO}_7:\text{Eu}^{2+}, \text{Dy}^{3+}$ phosphors were not irradiated by any excitation source such as UV, laser, X-ray, β -rays or γ -rays. The velocity of the moving piston, holding the impact mass could be changed (140–313 cm s^{-1}), by changing the height through which it was dropped [49]. In

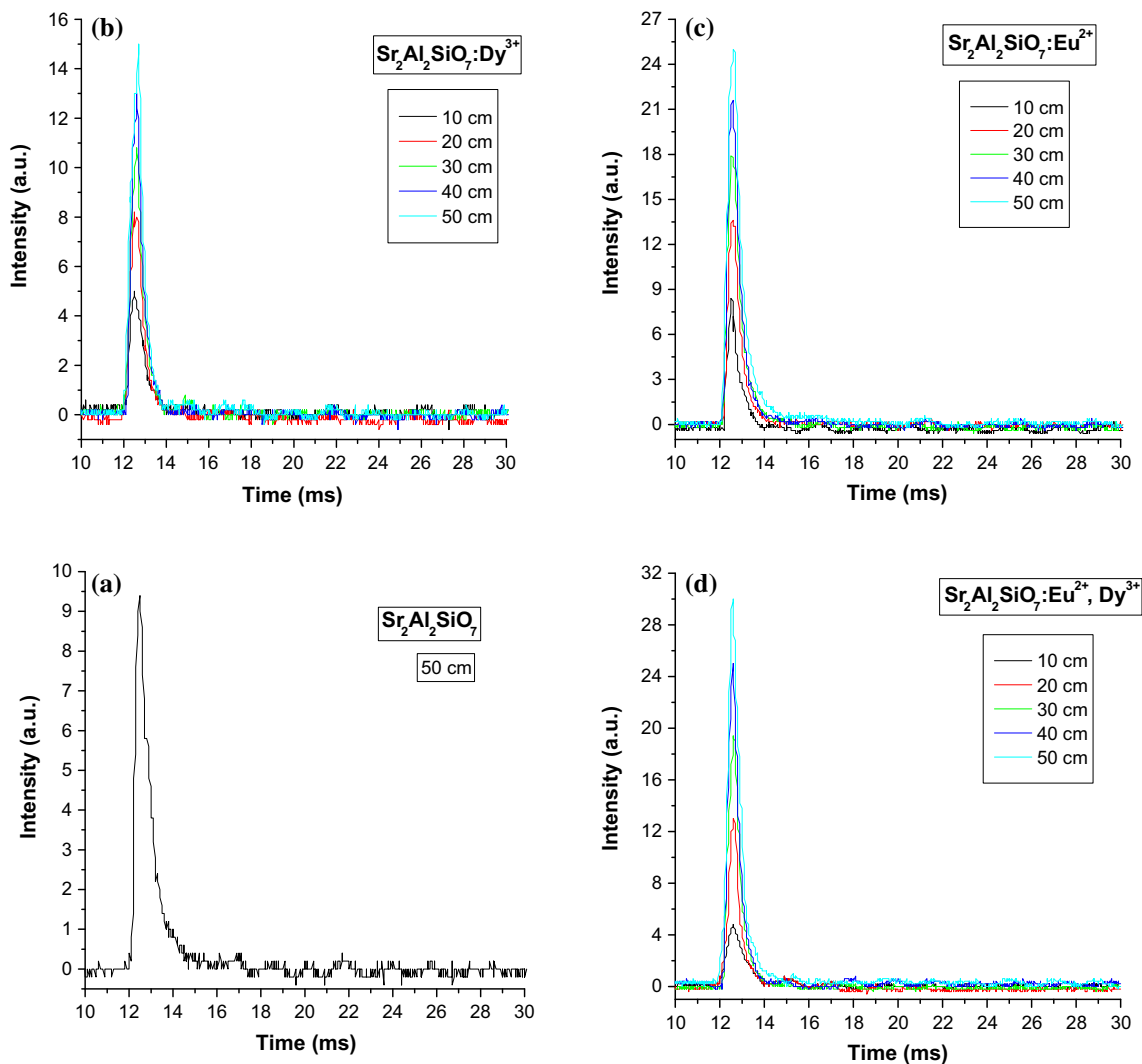


Fig. 11 ML intensity versus time curve of $\text{Sr}_2\text{Al}_2\text{SiO}_7$; $\text{Sr}_2\text{Al}_2\text{SiO}_7:\text{Dy}^{3+}$; $\text{Sr}_2\text{Al}_2\text{SiO}_7:\text{Eu}^{2+}$ and $\text{Sr}_2\text{Al}_2\text{SiO}_7:\text{Eu}^{2+}, \text{Dy}^{3+}$ phosphors

Fig. 11a, b, c, d ML curves measured by applying a load on the $\text{Sr}_2\text{Al}_2\text{SiO}_7$; $\text{Sr}_2\text{Al}_2\text{SiO}_7:\text{Eu}^{2+}$; $\text{Sr}_2\text{Al}_2\text{SiO}_7:\text{Dy}^{3+}$ and $\text{Sr}_2\text{Al}_2\text{SiO}_7:\text{Eu}^{2+}, \text{Dy}^{3+}$ phosphors dropped from heights 10, 20, 30, 40, and 50 cm respectively (there is no ML intensity has been obtain below the dropping height of 50 cm in $\text{Sr}_2\text{Al}_2\text{SiO}_7$ phosphor). In these ML measurements, the maximum ML intensity has been obtained for the 50 cm dropping height for $\text{Sr}_2\text{Al}_2\text{SiO}_7:\text{Eu}^{2+}$; $\text{Sr}_2\text{Al}_2\text{SiO}_7:\text{Dy}^{3+}$ and $\text{Sr}_2\text{Al}_2\text{SiO}_7:\text{Eu}^{2+}, \text{Dy}^{3+}$ phosphors, When the moving piston is dropped onto the prepared material at different height, light is emitted. The photon emission time is nearly 2 ms, when prepared material fractures. The strongest ML intensity could be obtained from Eu^{2+} doped and the Dy^{3+} co-doped $\text{Sr}_2\text{Al}_2\text{SiO}_7$ phosphor. However, from the ML glow curve, ML intensities are different for the different phosphors (see Figs. 11, 12). Figure 12 shows the comparative graph of ML intensity versus time of

$\text{Sr}_2\text{Al}_2\text{SiO}_7$; $\text{Sr}_2\text{Al}_2\text{SiO}_7:\text{Dy}^{3+}$; $\text{Sr}_2\text{Al}_2\text{SiO}_7:\text{Eu}^{2+}$ and $\text{Sr}_2\text{Al}_2\text{SiO}_7:\text{Eu}^{2+}, \text{Dy}^{3+}$ phosphors for 50 cm dropping height. The strongest ML intensity could be obtained in the order of $\text{Sr}_2\text{Al}_2\text{SiO}_7:\text{Eu}^{2+}, \text{Dy}^{3+} \gg \text{Sr}_2\text{Al}_2\text{SiO}_7:\text{Eu}^{2+} \gg \text{Sr}_2\text{Al}_2\text{SiO}_7:\text{Dy}^{3+} \gg \text{Sr}_2\text{Al}_2\text{SiO}_7$ phosphors.

Figure 13 shows the dependence of peak ML intensities on impact velocity of $\text{Sr}_2\text{Al}_2\text{SiO}_7:\text{Dy}^{3+}$; $\text{Sr}_2\text{Al}_2\text{SiO}_7:\text{Eu}^{2+}$ and $\text{Sr}_2\text{Al}_2\text{SiO}_7:\text{Eu}^{2+}, \text{Dy}^{3+}$ phosphors. The ML intensity increases linearly with the increases the falling height of the moving piston; that is, the ML intensity depends upon the impact velocity of the moving piston [$u_0 = \sqrt{2gh}$ (where h , is the different heights of moving piston)]. The ML intensity of $\text{Sr}_2\text{Al}_2\text{SiO}_7:\text{Dy}^{3+}$; $\text{Sr}_2\text{Al}_2\text{SiO}_7:\text{Eu}^{2+}$ and $\text{Sr}_2\text{Al}_2\text{SiO}_7:\text{Eu}^{2+}, \text{Dy}^{3+}$ phosphors increases with increasing the mechanical stress. The $\text{Sr}_2\text{Al}_2\text{SiO}_7:\text{Eu}^{2+}, \text{Dy}^{3+}$ phosphor possesses the strongest ML intensity as compare to $\text{Sr}_2\text{Al}_2\text{SiO}_7:\text{Dy}^{3+}$ and $\text{Sr}_2\text{Al}_2\text{SiO}_7:\text{Eu}^{2+}$

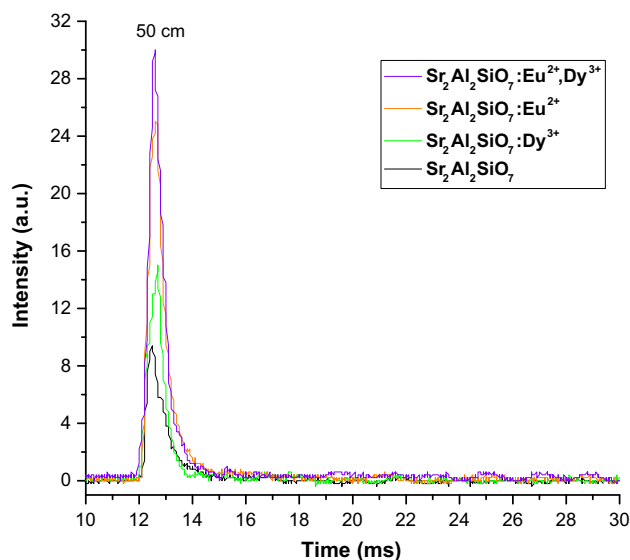


Fig. 12 Comparatively ML intensity versus time of $\text{Sr}_2\text{Al}_2\text{SiO}_7$; $\text{Sr}_2\text{Al}_2\text{SiO}_7:\text{Dy}^{3+}$; $\text{Sr}_2\text{Al}_2\text{SiO}_7:\text{Eu}^{2+}$ and $\text{Sr}_2\text{Al}_2\text{SiO}_7:\text{Eu}^{2+}, \text{Dy}^{3+}$ phosphors

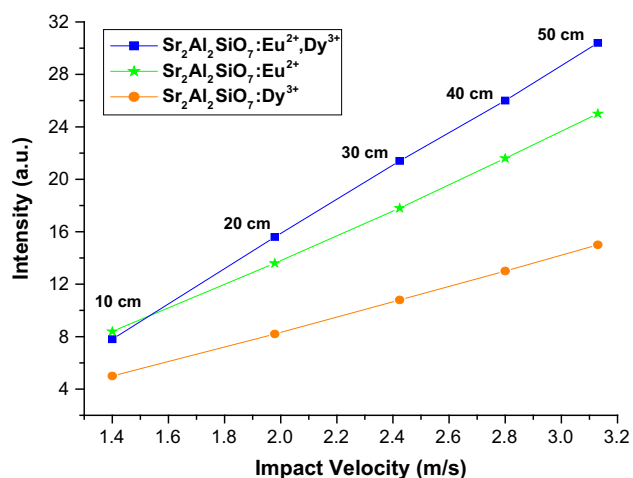


Fig. 13 ML intensity versus impact velocity curve of $\text{Sr}_2\text{Al}_2\text{SiO}_7:\text{Dy}^{3+}$; $\text{Sr}_2\text{Al}_2\text{SiO}_7:\text{Eu}^{2+}$ and $\text{Sr}_2\text{Al}_2\text{SiO}_7:\text{Eu}^{2+}, \text{Dy}^{3+}$ phosphors

phosphors. These properties indicate that this sample can be used as sensors to detect the stress of an object and self-diagnosis applications [54].

The ML intensity, which means peak ML intensity during force, strongly depended on the height of the moving piston. In addition, the PL intensity of $\text{Sr}_2\text{Al}_2\text{SiO}_7:\text{Eu}^{2+}, \text{Dy}^{3+}$ is about two orders of magnitude stronger than that of $\text{Sr}_2\text{Al}_2\text{SiO}_7:\text{Eu}^{2+}$, while the ML intensity of $\text{Sr}_2\text{Al}_2\text{SiO}_7:\text{Eu}^{2+}, \text{Dy}^{3+}$ phosphor increases only slightly. This suggests that Dy^{3+} ions sensitize the emission of Eu^{2+} ions more efficiently in a light-induced process than in a mechanical excitation process. The afterglow decay time of $\text{Sr}_2\text{Al}_2\text{SiO}_7:\text{Eu}^{2+}, \text{Dy}^{3+}$ phosphor is enhanced largely due to the existence of traps created by co-doped Dy^{3+} ions

(Fig. 9), which is similar to the change in ML intensity. This result indicates that the traps play as important a role in ML as they do in the long afterglow decay process.

For the ML in $\text{Sr}_2\text{Al}_2\text{SiO}_7$; $\text{Sr}_2\text{Al}_2\text{SiO}_7:\text{Eu}^{2+}$; $\text{Sr}_2\text{Al}_2\text{SiO}_7:\text{Dy}^{3+}$ and $\text{Sr}_2\text{Al}_2\text{SiO}_7:\text{Eu}^{2+}, \text{Dy}^{3+}$ phosphors, three mechanisms are possible: (1) charged dislocation model, (2) piezoelectrification induced electroluminescence model, and (3) local piezoelectricity-induced electron bombardment model. The charge dislocation model is not applicable because of these following experimental regions: (1) in elastic region the ML intensity of aluminate and silicate phosphors is repetitive, and (2) intense ML appears when the phosphor is placed in inside transparent illustrating liquid and hydrostatic pressure is applied. As the dislocations cannot move under hydrostatic pressure the dislocation origin of ML is not possible. In the case of phosphor in nanometer size the mean free path of de-trapped electrons is the order of the crystallite size, which is in the nanometer range. For such value of the mean free path the de-trapped electrons may not get sufficient energy for the impulsive excitation of luminescence centers. In fact, for the $\text{Sr}_2\text{Al}_2\text{SiO}_7$; $\text{Sr}_2\text{Al}_2\text{SiO}_7:\text{Eu}^{2+}$; $\text{Sr}_2\text{Al}_2\text{SiO}_7:\text{Dy}^{3+}$ and $\text{Sr}_2\text{Al}_2\text{SiO}_7:\text{Eu}^{2+}, \text{Dy}^{3+}$ phosphors of local piezoelectricity-induced electron bombardment model may be applicable.

When a mechanical stress, such as compress, friction, and striking, and so on, was applied on the sintered phosphors, piezo-electric field can be produced. Therefore, in such phosphor the ML excitation may be caused by the local piezoelectric field near the impurities and defects in the crystals. During the impact on the material, one of its newly created surfaces gets positively charged and the other surface of the crack gets negatively charged (see Fig. 14). Thus, an intense electric field of the order of $10^6\text{--}10^7 \text{ V cm}^{-1}$ is produced. Under such order of electric field, the ejected electrons from the negatively charged surface may be accelerated and subsequently their impact on the positively charged surfaces may excite the luminescence center [55]. Thus, depending on the prevailing conditions, recombination luminescence may be produced. For the impact velocity (v_0), the impact pressure P_0 will be equals to, $P_0 = Zv_0$, where Z is a constant. With increasing value of impact velocity, the depth of the trap will decrease, therefore, for the trap depth beyond a particular pressure the traps will be unstable and they will be de-trapped, in which the number of de-trapped electrons will increases with the increasing impact velocity. Thus, the ML intensity will increase proportionally with increasing value of impact velocity [56].

As the impact velocity increases, the impact pressure also increases leading to the increase in the electric field at local region which causes the decrease in trap depth. Hence the probability of de-trapping increases. From Fig. 13, it can be seen that with increasing impact velocity, ML intensity also increases linearly i.e., the ML intensity of $\text{Sr}_2\text{Al}_2\text{SiO}_7:\text{Dy}^{3+}$;

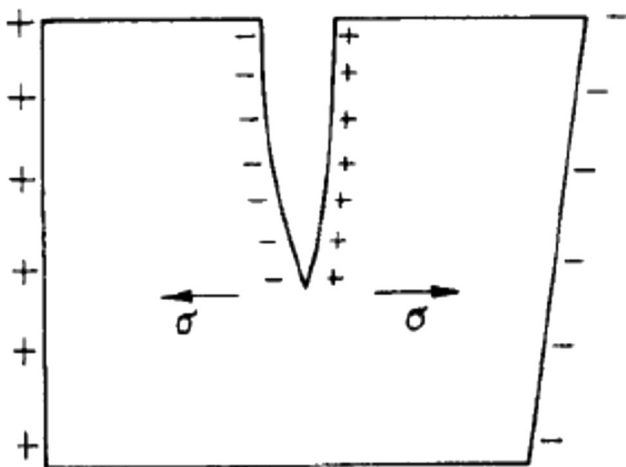


Fig. 14 Langevin model for the piezo-electrification induce phosphor

$\text{Sr}_2\text{Al}_2\text{SiO}_7:\text{Eu}^{2+}$ and $\text{Sr}_2\text{Al}_2\text{SiO}_7:\text{Eu}^{2+}, \text{Dy}^{3+}$ phosphors are linearly proportional to the magnitude of the impact velocity. When the surface of an object was coated with the ML materials, the stress distribution in the object beneath the layer could be reflected by the ML brightness and could be observed [57, 58]. Based on the above analysis this phosphor can also be used as sensors to detect the stress of an object. Thus the present investigation indicates that the piezo-electricity is responsible to produce ML in prepared $\text{Sr}_2\text{Al}_2\text{SiO}_7$; $\text{Sr}_2\text{Al}_2\text{SiO}_7:\text{Eu}^{2+}$; $\text{Sr}_2\text{Al}_2\text{SiO}_7:\text{Dy}^{3+}$ and $\text{Sr}_2\text{Al}_2\text{SiO}_7:\text{Eu}^{2+}, \text{Dy}^{3+}$ phosphors.

4 Conclusion

The $\text{Sr}_2\text{Al}_2\text{SiO}_7$; $\text{Sr}_2\text{Al}_2\text{SiO}_7:\text{Eu}^{2+}$; $\text{Sr}_2\text{Al}_2\text{SiO}_7:\text{Dy}^{3+}$ and $\text{Sr}_2\text{Al}_2\text{SiO}_7:\text{Eu}^{2+}, \text{Dy}^{3+}$ phosphors were synthesized by the traditional high temperature solid state reaction method. Chemical compositions of the sintered phosphors were confirmed by EDX spectra. The addition of co-dopant Dy^{3+} can increase the TL, PL, afterglow and ML intensity considerably. The new traps created by Dy^{3+} are responsible for this obvious increase. Under the UV excitation, the prepared $\text{Sr}_2\text{Al}_2\text{SiO}_7:\text{Dy}^{3+}$ phosphor would emit blue, yellow and red light with peak at 476, 578 and 675 nm corresponds to the transitions of $^4\text{F}_{9/2} \rightarrow ^6\text{H}_{15/2}$, $^4\text{F}_{9/2} \rightarrow ^6\text{H}_{13/2}$ and $^4\text{F}_{9/2} \rightarrow ^6\text{H}_{11/2}$ respectively. The three emission bands of the $\text{Sr}_2\text{Al}_2\text{SiO}_7:\text{Dy}^{3+}$ phosphor combines to give out white light, which was confirmed from the calculated CIE coordinates which were found to be very close to standard white light for human eyes. The $\text{Sr}_2\text{Al}_2\text{SiO}_7:\text{Eu}^{2+}$ and $\text{Sr}_2\text{Al}_2\text{SiO}_7:\text{Eu}^{2+}, \text{Dy}^{3+}$ phosphor emit the bluish-green emission which was again confirmed from the calculated CIE coordinates. It is worthy to note that the dependence between ML intensity of $\text{Sr}_2\text{Al}_2\text{SiO}_7:\text{Dy}^{3+}$; $\text{Sr}_2\text{Al}_2\text{SiO}_7:\text{Eu}^{2+}$ and $\text{Sr}_2\text{Al}_2\text{SiO}_7:\text{Eu}^{2+}, \text{Dy}^{3+}$ phosphors

and the impact velocity is close to linearity, which suggests these phosphors can also be used as sensors to detect the stress of an object.

Acknowledgments We are very much grateful to UGC-DAE Consortium for Scientific Research, Indore (M.P.) for the XRD Characterization and we are also very much thankful to Dr. Mukul Gupta for his co-operation.

References

1. N. Lakshminarasimhan, U.V. Varadaraju, Mater. Res. Bull. **43**, 2946–2953 (2008)
2. H.W. Leverenz, *An Introduction to Luminescence of Solids* (Dover Publications Inc., New York, 1968)
3. I.P. Sahu, D.P. Bisen, N. Brahme, M. Ganjir, Lumin. J. Biol. Chem. Lumin. (2015). doi:10.1002/bio.2869
4. H. Wu, Y. Hu, L. Chen, X. Wang, J. Alloys Compds. **509**, 4304–4307 (2011)
5. Y. Chen, X. Cheng, M. Liu, Z. Qi, C. Shi, J. Lumin. **129**, 531–535 (2009)
6. H. Wu, Y. Hu, G. Ju, L. Chen, X. Wang, Z. Yang, J. Lumin. **131**, 2441–2445 (2011)
7. S.H.M. Poort, W.P. Blokpoel, G. Blasse, Chem. Mater. **7**, 1547–1551 (1995)
8. R. Shrivastava, J. Kaur, Chin. Chem. Lett. (2015). doi:10.1016/j.ccllet.2015.05.028
9. K.Y. Jung, H.W. Lee, H.K. Jung, Chem. Mater. **18**, 2249–2255 (2006)
10. X.J. Li, Y.D. Qu, X.H. Xie, Z.L. Wang, R.Y. Li, Mater. Lett. **60**, 3673–3677 (2006)
11. H. Takasaki, S. Tanabe, T. Hanada, J. Ceram. Soc. Jpn **104**, 322–326 (1996)
12. H. Yamamoto, T. Matsuzawa, J. Lumin. **73**, 287–289 (1997)
13. I.P. Sahu, D.P. Bisen, N. Brahme, J. Radiat. Res. Appl. Sci. (2015). doi:10.1016/j.jrras.2015.02.007
14. M. Kimata, Z. Kristallogr. **167**, 103–116 (1984)
15. M. Merlini, M. Gemmi, G. Artioli, Z. Kristallogr. **Suppl.** **23**, 419–424 (2006)
16. Q. Zhang, J. Wang, M. Zhang, Q. Su, Appl. Phys. B **92**, 195–198 (2008)
17. X. Tan, J. Alloys Compds. **477**, 648–651 (2009)
18. C.N. Xu, T. Wantanabe, M. Akiyama, X.G. Zheng, Appl. Phys. Lett. **74**, 1236–1238 (1999)
19. I.P. Sahu, D.P. Bisen, R.K. Tamrakar, R. Shrivastava, Res. Chem. Intermed. (2015). doi:10.1007/s11164-015-2120-4
20. C.N. Xu, T. Wantanabe, M. Akiyama, X.G. Zheng, Appl. Phys. Lett. **74**, 2414–2416 (1999)
21. C.N. Xu, X.G. Zheng, M. Akiyama, K. Nonaka, T. Wantanabe, Appl. Phys. Lett. **76**, 179–181 (2000)
22. C.N. Xu, X.G. Zheng, T. Wantanabe, M. Akiyama, I. Usui, Thin Solid Films **352**, 273–278 (1999)
23. C. Zhao, D. Chen, Y. Yuan, M. Wu, Mater. Sci. Eng., B **133**, 200–204 (2006)
24. JCPDS file number 75-1234, JCPDS International Center for Diffraction Data
25. S. Basuna, G.F. Imbusch, D.D. Jiac, W.M. Yenc, J. Lumin. **104**, 283–294 (2003)
26. R. Chen, Y. Kirsh, Pergamon Press. Oxford **15**, 167 (1981)
27. F.M. Emen, N. Kulcu, A.N. Yazici, Eur. J. Chem. **1**(1), 28–32 (2010)
28. R. Chen, J. Appl. Phys. **40**(2), 570–585 (1969)
29. I.P. Sahu, D.P. Bisen, N. Brahme, Displays **38**, 68–76 (2015)
30. C.Y. Li, Q. Su, J.R. Qiu, Chin. J. Lumin. **24**, 19–27 (2003)

31. H.N. Luitel, T. Watari, R. Chand, T. Torikai, M. Yada, H. Mizukami, *Mater. Sci. Eng., B* **178**(12), 834–842 (2013)
32. T. Katsumata, R. Sakai, S. Komuro, T. Morikawa, *J. Electrochem. Soc.* **150**, H111–H114 (2003)
33. Z. Yuan, C. Chang, D. Mao, W. Ying, *J. Alloys Compd.* **377**(1–2), 268–271 (2004)
34. H. Kubo, H. Aizawa, T. Katsumata, S. Komuro, T. Morikawa, *J. Cryst. Growth* **275**(12), 1767–1771 (2005)
35. H. Wu, Y. Hu, B. Zeng, Z. Mou, L. Deng, *J. Phys. Chem. Solids* **72**, 1284–1289 (2011)
36. V. Pagonis, G. Kitis, C. Furetta, *Numerical and Practical Exercises in Thermoluminescence* (Springer, Berlin, 2006)
37. R. Chen, S.W.S. McKeever, *Theory of Thermoluminescence and Related Phenomenon* (World Scientific Press, Singapore, 1997)
38. M. Mashangva, M.N. Singh, T.B. Singh, *Indian J. Pure Appl. Phys.* **49**, 583–589 (2011)
39. G.S.R. Raju, J.Y. Park, H.C. Jung, B.K. Moon, J.H. Jeong, J.H. Kim, *Curr. Appl. Phys.* **9**(2), 92–95 (2009)
40. N.N. Yamashita, *J. Phys. Soc. Jpn.* **35**, 1089–1097 (1973)
41. A. Zukauskas, M.S. Shur, R. Gaska, *Introduction to Solid State Lighting* (Wiley, New York, 2002)
42. I.P. Sahu, D.P. Bisen, N. Brahme, *Displays* **35**, 279–286 (2014)
43. I.P. Sahu, D.P. Bisen, N. Brahme, M. Ganjir, *Lumin. J. Biol. Chem. Lumin.* (2015). doi:[10.1002/bio.2900](https://doi.org/10.1002/bio.2900)
44. CIE 1931. International Commission on Illumination. Publication CIE no. 15 (E-1.3.1) 1931
45. G. Blasse, B.C. Grabmarier, *Luminescent Materials* (Springer, Berlin, 1994), p. 96
46. I.P. Sahu, D.P. Bisen, N. Brahme, R.K. Tamrakar, *J. Radiat. Res. Appl. Sci.* **8**, 104–109 (2015)
47. R. Sakai, T. Katsumata, S. Komuro, T. Morikawa, *J. Lumin.* **85**, 149–154 (1999)
48. I.P. Sahu, D.P. Bisen, N. Brahme, R. Sharma, *Res. Chem. Intermed.* (2014). doi:[10.1007/s11164-014-1767-6](https://doi.org/10.1007/s11164-014-1767-6)
49. I.P. Sahu, D.P. Bisen, N. Brahme, L. Wanjari, R.K. Tamrakar, *Res. Chem. Intermed.* (2015). doi:[10.1007/s11164-015-1929-1](https://doi.org/10.1007/s11164-015-1929-1)
50. T. Aitasalo, J. Holsa, H. Jungner, M. Lastusaari, J. Niittykoski, *J. Phys. Chem. B* **110**, 4589–4598 (2006)
51. K.V.D. Eeckhout, P.F. Smet, D. Poelman, *Materials* **3**, 2536–2566 (2010)
52. D.R. Vijj, *Luminescence of Solids* (Plenum Press, New York, 1998)
53. B.P. Chandra, *J. Lumin.* **131**, 1203–1210 (2011)
54. I.P. Sahu, D.P. Bisen, N. Brahme, *Lumin. J. Biol. Chem. Lumin.* (2014). doi:[10.1002/bio.2771](https://doi.org/10.1002/bio.2771)
55. B.P. Chandra, R.A. Rathore, *Cryst. Res. Tech.* **30**, 885–896 (1995)
56. H. Zhang, H. Yamada, N. Terasaki, C.N. Xu, *Thin Solid Films* **518**, 610–613 (2009)
57. H. Zhang, H. Yamada, N. Terasaki, C.N. Xu, *Int. J. Mod. Phys. B* **23**, 1028–1033 (2009)
58. H. Zhang, H. Yamada, N. Terasaki, C.N. Xu, *Phys. E* **42**, 2872–2875 (2010)